



This is a repository copy of *Tactile Superresolution and Biomimetic Hyperacuity*.

White Rose Research Online URL for this paper:
<http://eprints.whiterose.ac.uk/92437/>

Version: Accepted Version

Article:

Lepora, N.F., Martinez-Hernandez, U., Evans, M. et al. (3 more authors) (2015) Tactile Superresolution and Biomimetic Hyperacuity. *IEEE Transactions on Robotics*, 31 (3). 605 - 618. ISSN 1552-3098

<https://doi.org/10.1109/TRO.2015.2414135>

Reuse

Unless indicated otherwise, fulltext items are protected by copyright with all rights reserved. The copyright exception in section 29 of the Copyright, Designs and Patents Act 1988 allows the making of a single copy solely for the purpose of non-commercial research or private study within the limits of fair dealing. The publisher or other rights-holder may allow further reproduction and re-use of this version - refer to the White Rose Research Online record for this item. Where records identify the publisher as the copyright holder, users can verify any specific terms of use on the publisher's website.

Takedown

If you consider content in White Rose Research Online to be in breach of UK law, please notify us by emailing eprints@whiterose.ac.uk including the URL of the record and the reason for the withdrawal request.



eprints@whiterose.ac.uk
<https://eprints.whiterose.ac.uk/>

Tactile hyperacuity for robotics

Nathan F. Lepora, Uriel Martinez-Hernandez, Mathew Evans, Lorenzo Natale, Giorgio Metta and Tony J. Prescott

Abstract—Hyperacuity is a general aspect of animal perception that exploits spatially overlapping sensory receptive fields to perceive at finer acuity than the sensor resolution. Following a recent demonstration of hyperacuity in robot touch, we present a detailed and systematic analysis of localization acuity for both a biomimetic fingertip and a region of tactile skin. We identify three key factors for hyperacuity: (i) the sensor is constructed with multiple overlapping, broad but sensitive receptive fields; (ii) the tactile perception method interpolates between receptors (taxels) to attain sub-taxel acuity; (iii) active perception ensures robustness to unknown initial contact location. All factors follow from active Bayesian perception applied to biomimetic tactile sensors based on a capacitive technology. In consequence, we attain extreme hyperacuity with a thirty-fold improvement of localization acuity (0.12mm) over sensor resolution (4mm). We envisage that these principles will enable cheap, high-acuity tactile sensors that are highly customizable to suit various applications in robot touch.

Index Terms—Force and tactile sensing, recognition, biomimetics, contact modelling.

I. INTRODUCTION

ALTHOUGH biological hyperacuity is most widely studied in vision [1], it also occurs for touch and audition, and may be considered a general aspect of human/animal perception. For example, Braille reading can involve perceiving spatial patterns of finer detail than the spacing between touch receptors in the human fingertip [2], [3]. No physical laws are broken because the perception involves spatial averages over the sensor distribution, which can transcend the resolution limit. Thus, nature has discovered design principles that allow perceptual systems to operate at finer acuity than might be expected from their sensory receptor densities. These principles give lessons for robotics when optimizing sensor performance.

In a recent study, we gave an initial demonstration of hyperacuity in robot touch [4] using a biomimetic fingertip [5] constructed for the iCub robot [6]. Originally, that study began as a demonstration that the fingertip could perceive the shape (curvature) and horizontal location of a rod by tapping down onto it. To our surprise, the localization acuity (~ 0.5 mm) was an order of magnitude better than the (4 mm) spacing of the tactile pixels (taxels). Investigating why, we noticed that

the design of the fingertip caused a contact over one taxel to activate its neighbors; moreover, the taxel readings were highly sensitive and decreased smoothly as a contact moved away from the taxel center. These principles are exactly those that enable biological systems to perceive at finer acuity than the sensor resolution (receptor spacing), which is a phenomenon called *hyperacuity*.

In this paper, we make a detailed and systematic analysis of localization hyperacuity for both the biomimetic fingertip [5] and a region of tactile skin [7] (an iCub palm [5]). To facilitate this analysis, we collect contact data at a high spatial sampling density (100 taps/mm) over a span that contains each sensor's entire location range (fingertip: 30 mm; skin: 50 mm). We can then characterize how localization acuity depends on the classification resolution for class widths $\gtrsim 0.1$ mm, a key variable for the degree of hyperacuity. A core component of our analysis is to compare methods for *active* and *passive* Bayesian perception [8] on the tactile dataset. We find that active perception is key to obtaining a high degree of hyperacuity, because it enables the sensor to relocate itself to a region of fine localization acuity. In consequence, we obtain *extreme* hyperacuity (0.12 mm acuity), with a thirty-fold improvement over sensor resolution.

These findings have implications both for the design of high acuity tactile sensors and the methods used for robot touch. A frequent assumption in tactile robotics is that 'more taxels are better' (or, equivalently, sensors with fewer taxels are criticized). However, we disagree. Perceptual acuity depends on a combination of factors, including taxel density, spatial layout, pressure sensitivity and receptive field size or shape, coupled with utilizing active and probabilistic methods for perception. Thus, to optimize sensor performance, constraints such as manufacturing costs and sensor robustness will necessitate a balance between these design factors, rather than focussing on any one in isolation. This balance will not necessarily involve having a high taxel density. For practical applications in future robotics, our expectation is that sensor optimization will be a sophisticated procedure, requiring modeling and empirical work to customize the design to suit a robot's intended use.

II. BACKGROUND AND RELATED WORK

A. Biological sensing and hyperacuity

Our senses, such as vision, audition and touch, take their inputs via sensory receptors that transduce stimuli from the physical world into signals appropriate for neural processing. For example, photoreceptors (vision) transduce light energy and mechanoreceptors (touch and audition) transduce kinetic energy into patterns of electrical spikes (*e.g.* [9], [10]). Each receptor has a receptive field, or region of space to which it responds, such as a cone of light rays onto a photoreceptor or

Manuscript submitted January 20, 2013. This work was supported in part by the European Commission under projects EFAA (ICT-270490) and WYSIWYD (ICT-612139).

N. Lepora is with the Department of Engineering Mathematics, The University of Bristol, and the Bristol Robotics Laboratory (BRL), The University of Bristol and the University of the West of England (UWE), Bristol, UK. (email: n.lepora@bristol.ac.uk)

U. Martinez-Hernandez, M. Evans and T. Prescott are with the Sheffield Center for Robotics (SCentRo), University of Sheffield, UK. (email: mat.evans@shef.ac.uk, uriel.martinez@shef.ac.uk, t.j.prescott@shef.ac.uk)

L. Natale and G. Metta are with the Department of Robotics, Brain and Cognitive Sciences, Italian Institute of Technology (IIT), 16163 Genova, Italy (e-mail: lorenzo.natale@iit.it, giorgio.metta@iit.it).

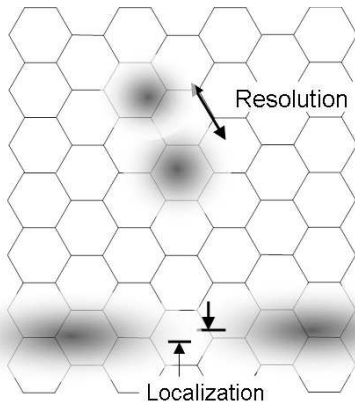


Fig. 1. Localization hyperacuity versus sensor resolution. Top: Two point-like (noisy) images on the mosaic of receptors can be resolved only if their separation leaves at least one intervening receptor with a detectably different intensity. Bottom: Two targets can be localized relative to each other to finer acuity than the receptor spacing; the hyperacuity mechanism achieves this by identifying the center of each target across all of the receptors it covers. (Image reproduced from [11] under the creative commons license.)

a patch of skin activating a mechanoreceptor. For our senses to cover their nearby environment, receptors are packed together into mosaic-like arrays. The spacing between receptors then defines the sensor resolution, and relates to the minimum separation to distinguish two point-like stimuli (Fig. 1). For a healthy human eye, the angular resolution is about 1 arcmin (0.02 degs), or 30 cm at 1 km distance; for a human fingertip, the two-point discrimination is about 3 mm on the skin [2].

Acuity is the sharpness of perception, and depends on both the sensory apparatus and the computations underlying perception. Measures of acuity rely on quantifying the finest discriminable detail of a stimulus, such as reading letters on the lowest line of a Snellen chart at 20 feet distance (called 20/20 vision). More formally, acuity can be defined as $1/RP$, where RP is the resolving power given by the angle (vision) or distance (touch) spanned by the detail; a visual RP of 1 arcmin is considered normal and defines 20/20 vision.

Hyperacuity is a perceptual effect where the resolving power of the stimulus detail is finer than the sensor resolution [1]. It has been studied primarily for human visual localization, where the parallel encoding of a stimulus across multiple sensory receptors is known to aid computation of population averages with finer acuity than the sensor resolution (Fig. 1). Visual hyperacuity has been observed for curvature detection, edge smoothness, stereoacuity (depth) and Vernier acuity (alignment of two parallel lines). The highest hyperacuity measured with the human eye was the relative position of a line to 0.85 arcsec (0.0002 degs), equivalent to 4 mm at 1 km [12].

Human touch is also known to attain hyperacuity [2]: for static (~ 1 sec) touches against embossed spatial patterns, subjects estimated relative interval size to 0.3 mm and (modified Vernier) alignment to 0.4 mm. Both measurements are an order of magnitude better than the two-point discrimination interval (~ 3 mm) and the average spacing ($\sim 70/\text{cm}^2$) between (SA-I) mechanoreceptors in the fingertip. Practical benefits include Braille reading, which can involve sub-millimeter judgments of surface detail that depend upon tactile hyperacuity [2], [3].

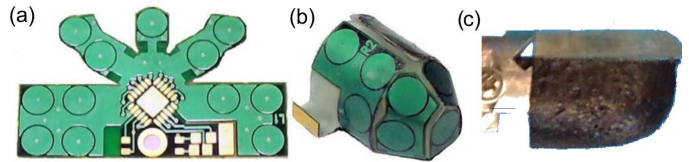


Fig. 2. Construction of tactile fingertip. A flexible PCB (a) is wrapped around a hard core (b) then covered in a soft silicon foam insulator and conductive rubber (c) to give a capacitive touch sensor. The lower plates of the 12 taxels are visible as circles on the PCB. (Figure adapted from [5].)

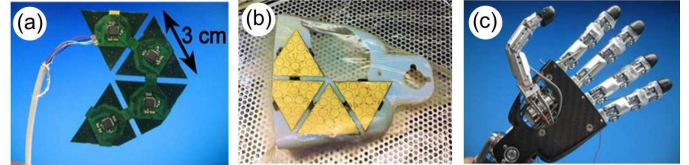


Fig. 3. Construction of region of tactile skin. A flexible PCB (a) is mounted on a solid base (b) then covered in a soft silicon foam insulator and conductive fabric (c) to give a touch sensitive palm. (Figure adapted from [5].)

B. Artificial hyperacuity and robot tactile perception

Implementing hyperacuity with artificial sensors has been confined mainly to visual imaging, where it is known as *super-resolution*, or more precisely *geometrical superresolution* [13]. Examples include sub-pixel localization [14] from interpolating over pixel distributions, and multi-exposure noise reduction [15] by averaging several images. One should be careful to distinguish these methods from *optical super-resolution* [16], which is concerned with transcending the diffraction limit rather than the resolution limit [13]. Advances in super-resolution technology are impacting science from cell biology to medical imaging ‘in ways unthinkable in the mid-90s’ [17] and were honored as a Nature ‘method of the year’ [18].

An initial demonstration of hyperacuity in robot touch [4] has been implemented with a biomimetic fingertip [5] mounted on a Cartesian robot. Using a taxel-based sensor design (Fig. 2), a cylindrical stimulus could be localized to ~ 0.5 mm, an order of magnitude better than the 4 mm taxel spacing. That study also found that active perception helped the hyperacuity, although the methods suffered (in hindsight) from being somewhat *ad hoc* and did not use location information to control the sensor. Further, the tactile dataset was taken over a somewhat narrow location range (16 mm) with a sampling density (320 taps) consistent with a class resolution of 1 mm, which was wider than the attained acuity. These issues are addressed in the current study, along with presenting a more principled and systematic analysis of artificial tactile hyperacuity.

The present and previous implementations of artificial tactile hyperacuity are built on two key principles: (i) the *sensors* are designed with taxels having broad but sensitive receptive fields; (ii) the *method* of Bayesian perception [4], [19], [20] can exploit this stimulus encoding to attain localization hyperacuity. Bayesian perception is grounded in optimal decision making in statistics and perceptual neuroscience [20], notably models of the basal ganglia and cortex in perceptual decision making [21], [22]. Hence, we think it reasonable to claim that our method for implementing hyperacuity in artificial systems mirrors the principles used in biological perception.

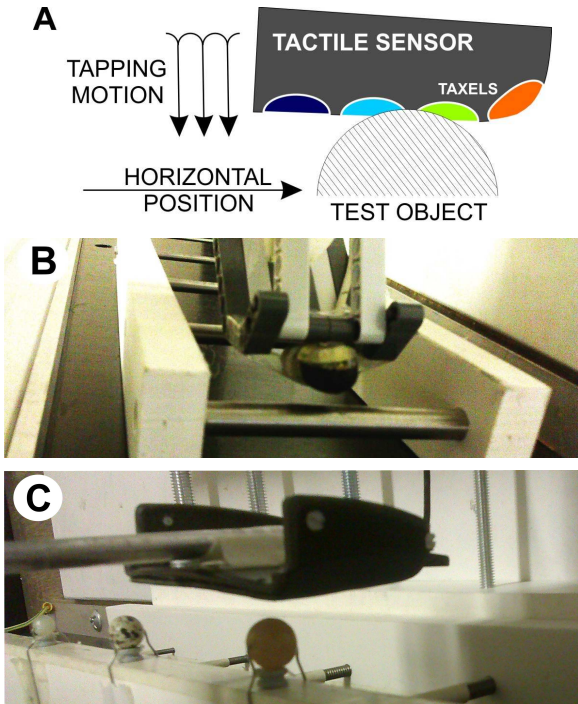


Fig. 4. Experimental setup. (A) Schematic of tactile sensor tapping against a cylindrical test object, with the pressure-sensitive taxels (colored) impinging onto the test object. For collecting training data, each tap is then followed by a small horizontal move to span the entire location range. (B) Forward view of the mounted fingertip tapping against a steel rod. (C) Side view of the tactile skin mounted on the Cartesian robot tapping against a sphere. These experimental setups are ideal for systematic data collection to characterize the properties of the sensor interacting with objects.

III. MATERIALS AND METHODS

A. Tactile robots and experiments

Two tactile sensors are used in this study (Figs 2,3) that were designed originally as a tactile fingertip [5] and skin (palm) [7] for the iCub humanoid robot. The two tactile sensors are of a size commensurate with a human infant, in keeping with the design of the iCub [6]. The tactile fingertip has a rounded shape of dimensions 14.5 mm long by 13 mm wide (Fig. 2A), covered with $N_{\text{taxels}} = 12$ pressure sensitive taxels. The tactile skin has 4 equilateral triangular-shaped taxel arrays in a flat layout, each 30 mm wide and covered with 12 taxels, giving $N_{\text{taxels}} = 48$ total (Fig. 2B). These tactile sensors detect pressure by the capacitance change due to a compressible insulating layer between the inner conducting plate of the taxels and an electrically conductive outside layer. The two sensors have a similar design for the inner conducting plates (a flexible PCB) and insulating layer (soft silicone foam, 2 mm deep), but differ in their outside layer: the fingertip uses conductive silicone rubber, whereas the skin uses conductive Lycra-like fabric. For more details of their construction, we refer to the original reference on the technologies for the implementation of large-scale robot tactile sensors [5], [7].

Here we mount each tactile sensor as an end effector on a two degree-of-freedom Cartesian robot (2-axis PXYx, Yamaha Robotics). This combination of tactile sensor with Cartesian robot has been employed previously for testing various tactile sensors, including tactile vibrissae [23], [24]

and tactile fingertips [4], [8], [25]–[27]. The Cartesian robot has the benefit that it can precisely position the sensor in a two-dimensional plane ($\sim 20 \mu\text{m}$ accuracy) with excellent repeatability. As such, it is an ideal platform to probe tactile sensing; for example, by tapping the sensor against various test objects over a systematic and exhaustive range of locations.

The present study focusses on the tangential localization acuity of a curved object impinging against the tactile sensor surface. Both types of tactile sensor were mounted with their (horizontal) sensing surface oriented approximately perpendicular to the (vertical) direction of the tapping motion (Fig. 4A). For the fingertip, a smooth steel cylindrical rod (diameter 8 mm) was used as a test object (Fig. 4B). For the skin, a smooth spherical stone ball (diameter 8 mm) was used (Fig. 4C). In both cases, the perceptual task is to determine the tangential (horizontal) localization of the test object by tapping against it.

Touch data were collected while the tactile sensor tapped vertically onto and off the test object, followed by a horizontal move Δx across the closest face of the object before making the next tap (Fig. 2A). For the fingertip, a horizontal x -range of 30 mm was used with a move $\Delta x = 0.01$ mm, giving 3000 taps across the cylindrical object. For the skin, a horizontal x -range of 50 mm was used with a move $\Delta x = 0.01$ mm, giving 5000 taps across the spherical object. From each tap of a tactile sensor against the test object, a 1 sec time series of pressure readings ($N_{\text{samples}} = 50$) was extracted for all N_{taxels} taxels. A 1 sec pause was taken between brief (~ 0.1 sec) contacts to ensure transients decayed; no noticeable hysteresis then occurred. Data were collected at 8 bit resolution and then high-pass filtered and normalized [5]. All data were collected twice to give distinct training and test sets.

B. Bayesian perception for robotics

We use a Bayesian perception method for classifying object location that is based on sequential analysis models of perceptual decision making in neuroscience and psychology [22], [28]. Sequential analysis is a statistical technique for hypothesis selection over data that is sequentially sampled until reaching a stopping condition [29], which commonly takes the form of a threshold on the posterior belief. Its application to neuroscience and psychology rests on the empirical success in modeling behavioral experiments (*e.g.* reaction time distributions) and also that neuronal activity during decision making is consistent with a threshold crossing. Theoretically, hypothesis selection via a belief threshold is known to optimize decision making under some circumstances (*e.g.* two choices with a linear cost function of decision time and error rate).

This Bayesian perception approach has been applied successfully to robot tactile perception [4], [8], [19], [20], [25]–[27]. The method implements a recursive Bayesian update of the posterior beliefs for each distinct perceptual class (the statistical hypotheses) until reaching a predefined decision threshold. Here we consider two implementations of Bayesian perception (Fig. 5), termed active and passive, depending on whether or not the sensor can relocate during perception. Although we here apply these methods to purely localization decisions, they have more general applicability [8].

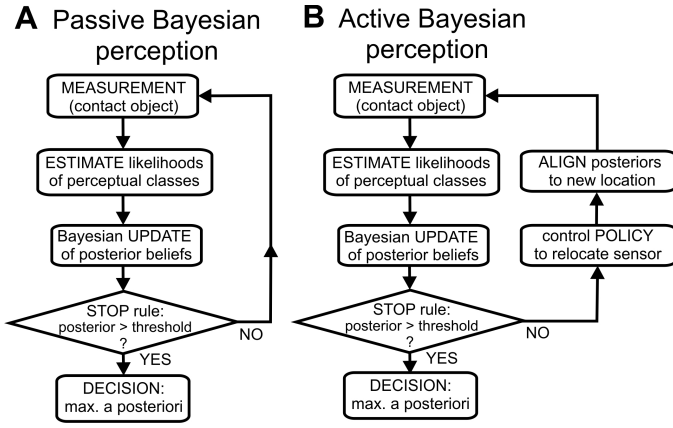


Fig. 5. Passive and active Bayesian perception. (A) Passive Bayesian perception has a recursive belief update with decision termination when the posterior belief reaches threshold. (B) Active Bayesian perception has the same recursive belief update, while also controlling sensor location according to a belief-based control policy. Upon moving the sensor, the location components of the posterior beliefs are re-aligned with the new sensor location. The two algorithms differ only in the control loop for active Bayesian perception.

Passive Bayesian perception accumulates belief for N_{loc} distinct location classes x_l by making successive taps z_t against a test object until at least one of the posterior location beliefs $P(x_l|z_{1:t})$ crosses a belief threshold θ_{dec} , when the localization decision x_{dec} is made. The passive nature of the perception means that the location class x_l is constant over the decision making process (Fig. 5A).

Active Bayesian perception also accumulates belief for the location classes x_l by successively tapping until a posterior belief $P(x_l|z_{1:t})$ reaches a predefined belief threshold θ_{dec} , but in addition utilizes a posterior-dependent control policy π to move the sensor during the perceptual process (Fig. 5B). Here we use a ‘fixation point’ control policy (Fig. 6) that infers a best estimate of current location x_{est} from the location beliefs, then calculates a relative move to a preset fixation position x_{fix} on the object. Provided the fixation point is a good location for perception, this control policy can progressively improve the perception during the decision making process from an initially unknown location (e.g. Fig. 7B).

Formally, the Bayesian perception method applies to sequences of contact data $z_{1:t} = \{z_1, \dots, z_t\}$, each of which is a multi-dimensional time series of sensor values,

$$z_t = \{s_k(j) : 1 \leq j \leq N_{samples}, 1 \leq k \leq N_{taxels}\}, \quad (1)$$

with indices j, k labeling the time samples and sensor taxels respectively. This contact data gives evidence for the present location class x_l , $1 \leq l \leq N_{loc}$, computed through the

b	bin index	N_{bins}	number of bins	s	sensor value	$z_{1:t}$	contact history to time t
e_{dec}	location error	N_{loc}	number of locations	t	time index	z_t	contact at time t
$h(b, k, l)$	sample histogram	$N_{samples}$	number of samples	t_{dec}	decision time	π	movement policy
I_b	bin interval	N_{taxels}	number of taxels	x_l	location class	θ_{dec}	decision threshold
j	sample index	$P(x_l z_{1:t})$	location belief	x_{est}	estimated location	θ_{est}	intermediate threshold
k	taxel index	$P(z_t x_l)$	location likelihood	x_{dec}	decided location		(0 for active; 1 for passive perception)
l	location index	$P(z_t z_{1:t})$	marginal probability	x_{fix}	fixation location		

TABLE I
SYMBOLS GLOSSARY.

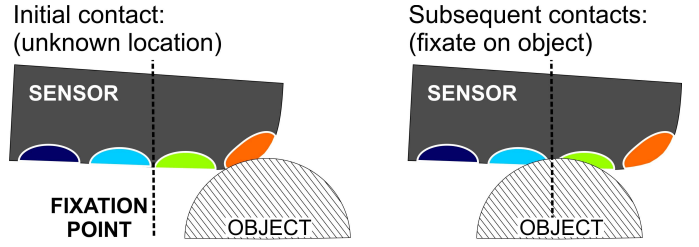


Fig. 6. Fixation point active control policy. The policy calculates a relative move to a preset fixation position x_{fix} on the object using a best estimate of current location x_{est} from the location beliefs. Provided the fixation point is a good location for perception, this control policy can progressively improve the perception during the decision making process.

algorithms in Fig. 5, with details as follows.

1) *Measurement model and likelihood estimation*: The location likelihoods $P(x_l|z_t)$ are found using a measurement model of the contact data, based on a histogram method applied to sampling distributions from training data over the distinct location classes [20], [30]. First, sensor values s_k for taxel k are binned into equal intervals I_b , $1 \leq b \leq N_{bins}$, with sampling distribution given by the normalized histogram $h(b, k, l)$ over all training data for each location class x_l :

$$P(b|k, l) = \frac{h(b, k, l)}{\sum_{b=1}^{N_{bins}} h(b, k, l)}, \quad (2)$$

where $h(b, k, l)$ is the sample count in bin b for taxel k over all training data in class x_l . Then, given a test contact z_t with samples $s_k(j)$, we construct a measurement model from the mean log likelihood over all samples in that contact

$$\log P(z_t|x_l) = \sum_{k=1}^{N_{taxels}} \sum_{j=1}^{N_{samples}} \frac{\log P(b_k(j)|k, l)}{N_{samples} N_{taxels}}, \quad (3)$$

where $b_k(j)$ is the bin occupied by sample $s_k(j)$. Technically, this measurement model becomes ill-defined if any histogram bin is empty, which is easily fixed by regularizing the bin counts with a small constant ($\epsilon \ll 1$), giving $h(b, k, l) + \epsilon$.

2) *Bayesian belief update*: Bayes’ rule is used after each successive test contact z_t to recursively update the posterior location beliefs $P(x_l|z_{1:t})$ for the perceptual classes with the location likelihoods $P(z_t|x_l)$ of that contact data

$$P(x_l|z_{1:t}) = \frac{P(z_t|x_l)P(x_l|z_{1:t-1})}{P(z_t|z_{1:t-1})}, \quad (4)$$

from background information given by the prior location beliefs $P(x_l|z_{1:t-1})$ (i.e. the posterior beliefs from the preceding contact). The marginal probabilities $P(z_t|z_{1:t-1})$ of the current

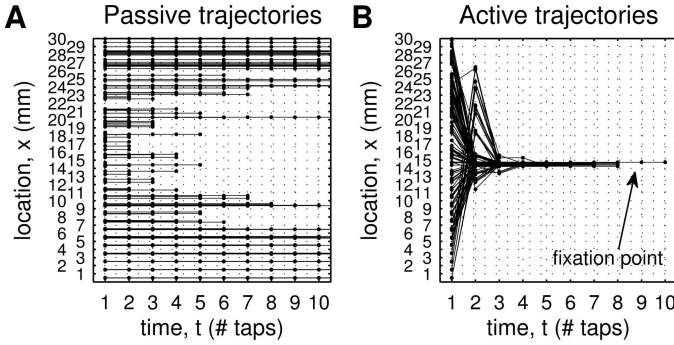


Fig. 7. Example trajectories for passive and active perception. 100 trajectories were selected randomly for each case ($\theta_{\text{dec}}=0.95$). (A) Passive perception, with sensor location constant over time. (B) Active perception, with trajectories converging on the central fixation point independent of starting position.

contact given the prior contact history are also conditioned on the preceding contacts $z_{1:t-1}$ and given by

$$P(z_t|z_{1:t-1}) = \sum_{l=1}^{N_{\text{loc}}} P(z_t|x_l)P(x_l|z_{1:t-1}). \quad (5)$$

Iterating (4,5), a sequence of contacts z_1, \dots, z_t results in a sequence of posterior beliefs $P(x_l|z_1), \dots, P(x_l|z_{1:t})$ initialized from uniform prior beliefs $P(x_l|z_0) := P(x_l) = 1/N_{\text{loc}}$.

3) *Final location decision*: Here we follow sequential analysis methods for optimal decision making that recursively update beliefs up to a threshold θ_{dec} that triggers the final decision (Fig. 8A). Thus, the update (4,5) stops when the posterior location belief $P(x_l|z_{1:t})$ passes a threshold θ_{dec} , giving a final location decision x_{dec} from the maximal *a posteriori* (MAP) estimate at time t_{dec}

$$\text{if any } P(x_l|z_{1:t}) > \theta_{\text{dec}} \text{ then } x_{\text{dec}} = \arg \max_{x_l} P(x_l|z_{1:t}). \quad (6)$$

This belief threshold θ_{dec} is a free parameter that adjusts the balance between decision time t_{dec} and accuracy e_{dec} . For a choice between two outcomes this speed-accuracy balance can be proved optimal [29]; optimality is not known for the many perceptual choices considered here, so we make a reasonable assumption of near optimality [20].

4) *Online re-location estimate*: Analogously to the stop decision, a sensor move requires a location belief to cross its own decision threshold [8], with the MAP estimate giving an intermediate location estimate for use in controlling the sensor

$$\text{if any } P(x_l|z_{1:t}) > \theta_{\text{est}} \text{ then } x_{\text{est}} = \arg \max_{x_l} P(x_l|z_{1:t}). \quad (7)$$

Here we consider two particular cases (Figs 5A,B), termed:

- (A) passive perception: $\theta_{\text{est}} = 1$ (never moves)
- (B) active perception: $\theta_{\text{est}} = 0$ (always tries to move).

For simplicity, we consider a control policy π for moving the sensor $x \leftarrow x + \pi(x_{\text{est}})$ that depends only on present estimated location x_{est} . Upon performing the resulting move, the location beliefs $P(x_l|z_{1:t})$ should then be kept aligned with

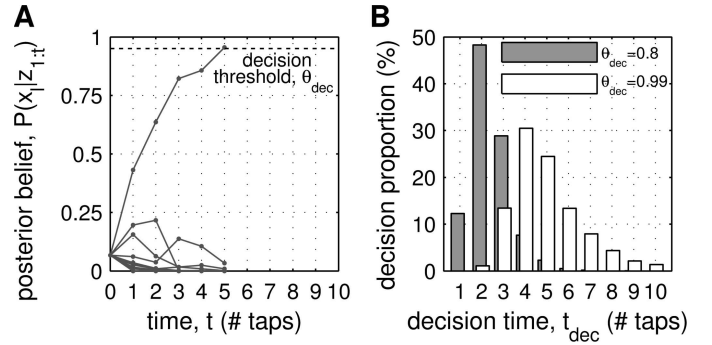


Fig. 8. Effect of decision threshold on perception. (A) Example decision, with evidence integrated over successive taps until a location belief crosses the decision threshold. (B) Histograms of decision times across many decisions; the distribution peak shifts to longer decision times for increased thresholds.

the sensor by shifting them by the number of classes moved

$$\begin{aligned} &\text{if } 1 \leq x_l - \pi(x_{\text{est}}) \leq N_{\text{loc}} \text{ then} \\ &\quad P(x_l|z_{1:t}) \leftarrow P(x_l - \pi(x_{\text{est}})|z_{1:t}), \\ &\text{if } x_l - \pi(x_{\text{est}}) < 1 \text{ or } x_l - \pi(x_{\text{est}}) > N_{\text{loc}} \text{ then} \\ &\quad P(x_l|z_{1:t}) \leftarrow p_0, \end{aligned} \quad (8)$$

where we recalculate the beliefs p_0 lying outside the original range by assuming they are uniformly distributed and the shifted beliefs $P(x_l|z_{1:t})$ sum to unity. The left arrow denotes that the quantity on the left is replaced with that on the right.

5) *Active control policy*: The final component of the active perception algorithm is to define the control policy for moving the sensor based on the posterior beliefs. For simplicity, here we consider a ‘fixation point’ policy motivated by orienting movements in animals: the control policy attempts to move the sensor to a predefined fixation point x_{fix} relative to the object assuming it is at the estimated location x_{est} on the object,

$$x \leftarrow x + \pi(x_{\text{est}}), \quad \pi(x_{\text{est}}) = x_{\text{fix}} - x_{\text{est}}, \quad (9)$$

where x is the actual (unknown) location of the sensor. In practice, only the move $\pi(x_{\text{est}})$ need be found, to instruct the sensor how to change relative location. Example trajectories resulting from this active control strategy are shown in Fig. 7B. Provided the fixation point is set to be a good location for perception, this control policy can progressively improve the perception during the decision making process from an initially unknown location where the perception may be poor.

C. Virtual environment estimate of location acuity

The aim of our data collection is to set up a ‘virtual environment’ in which methods for perception can be compared off-line on identical data. This is achieved by measuring contact signals over an exhaustive range of object locations. We can then use Monte Carlo validation to ensure good statistics: perceptual errors are averaged over many test runs with contact data drawn randomly from the perceptual classes (typically 10000 runs per data point plotted in the results).

For analysis, the data were separated into N_{loc} distinct classes, by collecting groups of contact data each spanning part of the overall range. For the tactile fingertip, we considered 10, 15, 30, 60, 100, 150, 300 location classes spanning

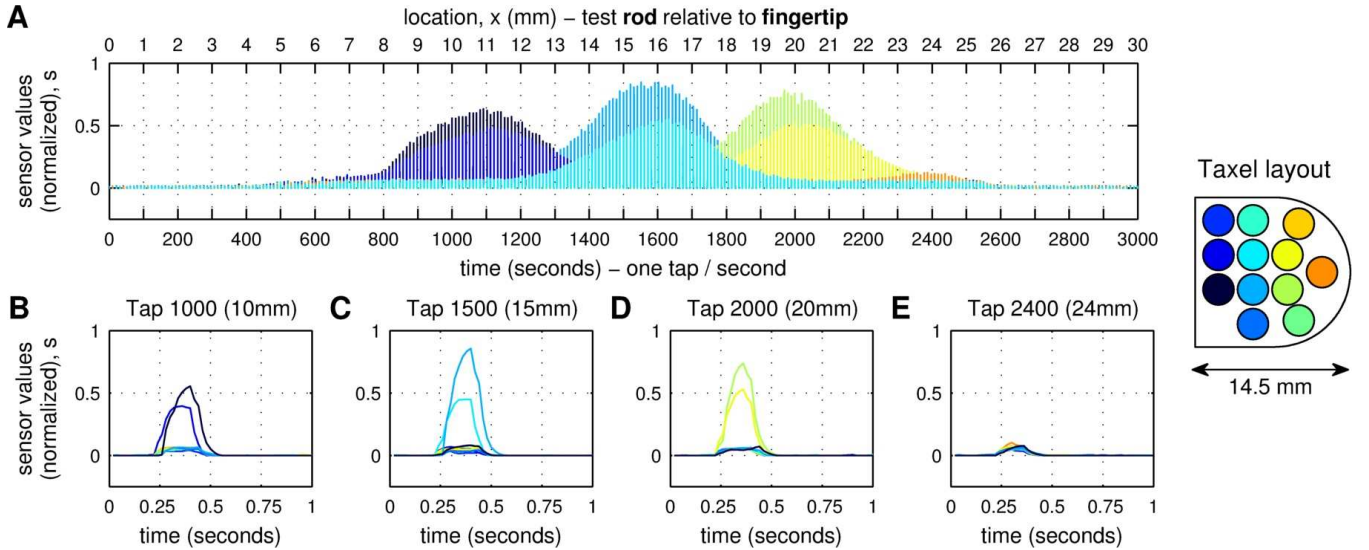


Fig. 9. Tactile data. Collected as the fingertip taps against a test rod (dia. 8 mm) at constant rate of 1 tap/second, with 0.01 mm displacement after every tap to span a 30 mm location range with 3000 taps. (B-E) Individual tap data taken from panel (A). Taxels are colored according to their layout on the fingertip.

a 30 mm range (class widths 3, 2, 1, 0.5, 0.3, 0.2, 0.1 mm). For the tactile skin, we considered 25, 50, 100, 200, 250, 500 location classes spanning a 50 mm range (class widths 2, 1, 0.5, 0.25, 0.2, 0.1 mm). The localization decision error e_{dec} was then quantified with the mean absolute error (MAE) $|x - x_{\text{dec}}|$ between the actual x and classified values x_{dec} of object location over all test runs.

Perceptual acuity can then be defined as the maximum of the mean localization error e_{dec} and the class width. For large class widths (small N_{loc}), the mean error is less than the class width, so the class width limits the perception; for small classes (large N_{loc}), the error is larger than the class width, and the localization error limits the perception.

IV. RESULTS

A. Tactile fingertip

1) *Inspection of data:* Data for the tactile fingertip (Fig. 9) were collected while the sensor tapped vertically onto and off the test object (cylindrical rod, 8 mm diameter). Each tap was followed by a horizontal move across the closest face of the rod before making the next tap to sample across a 30 mm position range. The initial and final parts of the data collection are for contacts either at the fingertip’s non-sensitive base or missing the object entirely, with little or no tactile response. Between these extremes, the first sensed contacts are with the taxels at the sensor’s base, followed by the middle taxels and finally the taxels at its tip. Each taxel has a broad, Gaussian-shaped receptive field about 8 mm across with centers spaced

about every 4 mm (Fig. 9A). Individual taps typically take ~ 0.1 sec to reach peak amplitude, followed by a rapid decay to baseline (Figs 9B-E). Hence, contact features from the stimulus are encoded both in the time-series response of each taxel and in which taxels are activated.

The most obvious effect of varying horizontal contact location of the fingertip against the object was a change in taxel identity and peak response amplitude. For each contact, the pattern of taxel pressures depends on the location of the fingertip relative to the object, permitting classification of where the rod is located relative to the fingertip. The geometry of the overlapping receptive fields implies that multiple taxels are activated simultaneously, so that the contacted stimuli are coarse-coded over multiple sensor outputs. We will see that these aspects of the data are important for the perceptual acuity of localizing the object being sensed.

2) *Passive Bayesian perception:* The perceptual acuity of the fingertip for locating the rod is assessed first with a passive Bayesian method for robot perception. Bayesian perception updates the posterior beliefs $P(x_l|z_{1:t})$ for N_{loc} distinct location classes x_l , using successive taps z_1, \dots, z_t against a test object until at least one belief crosses a decision threshold θ_{dec} . Results are generated with a Monte Carlo procedure using the data as a virtual environment (Sec. III-C), such that each contact tap *passively* remains at its initial location class (example trajectories in Fig. 8A).

Passive perceptual decisions of object location are evaluated for decision thresholds θ_{dec} from 0-0.999, over $N_{\text{loc}} = 30$

number of classes, N_{loc}	10	15	30	60	100	150	300
class width, x_{class}	3 mm	2 mm	1 mm	0.5 mm	0.3 mm	0.2 mm	0.1 mm
mean decision error, \bar{e}_{dec} (passive perception)	4.5 mm	4.5 mm	4.5 mm	4.5 mm	4.5 mm	4.5 mm	4.5 mm
mean decision error, \bar{e}_{dec} (active perception)	0 mm	0 mm	0.01 mm	0.04 mm	0.07 mm	0.08 mm	0.12 mm
acuity, $\max(x_{\text{class}}, \bar{e}_{\text{dec}})$ (active perception)	3 mm	2 mm	1 mm	0.5 mm	0.3 mm	0.2 mm	0.12 mm

TABLE II

ACTIVE PERCEPTUAL ACUITY DEPENDS ON LOCATION CLASS WIDTH. RESULTS ARE FOR MEAN DECISION TIMES OF 2 TAPS.

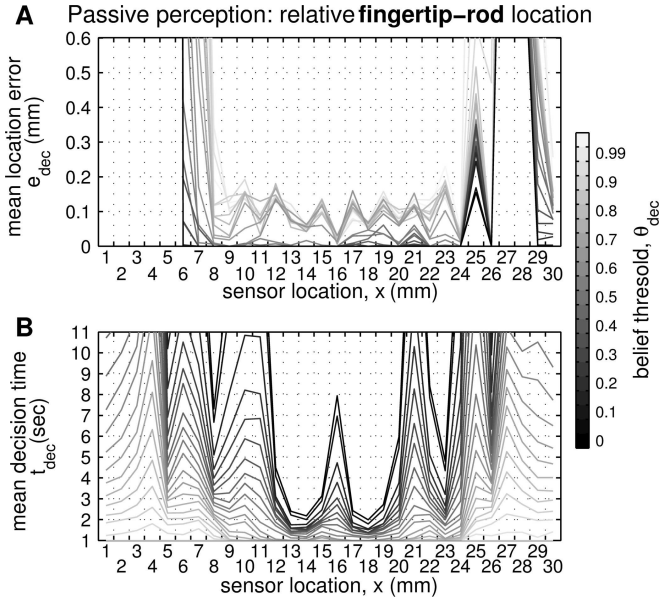


Fig. 10. Acuity of passive Bayesian perception depends on relative fingertip-rod location and belief threshold. (A) Mean location errors e_{dec} and (B) mean decision times t_{dec} plotted against sensor location x , with the gray-scale denoting the belief threshold (10000 trials per threshold value, with $N_{\text{loc}} = 30$ location classes). Perceptual performance is best in the central region of the location range and for higher belief thresholds.

location classes spanning the 30 mm range across the fingertip (Fig. 10). Perceptual error depends strongly on test location class, with mean location decision error e_{dec} increasing sharply at the extremes of the horizontal range from small errors in the central region (Fig. 10A). The lowest errors $e_{\text{dec}} \lesssim 0.2$ mm are in the region nearby the mid-point $x = 15$ mm of the 30 mm range. Decision times are modified from a U-shaped function (Fig. 10B), by also having a central spike that coincides with the maximum of the middle taxel’s receptive field (similar spikes also occur for adjacent taxels at 10 mm and 20 mm). Our interpretation of this effect is that the speed of perception is aided by spatial gradients in the taxel receptive fields; meanwhile, the overall U-shaped function of accuracy is consistent with contacts at the extremities being weak or non-existent with poor signal-to-noise ratio.

For passive perception, there is no control over the location from where an object is sensed. Hence, we typify the location accuracy for the fingertip and rod as a mean \bar{e}_{dec} over all possible sensing locations (Fig. 11A, red plot). Given $\bar{e}_{\text{dec}} \sim 4.5$ mm, this gives a poor location acuity dominated by the poor perception on the extremities of the range. These results emphasize that passive perception performs poorly because it cannot control contact location.

3) *Active Bayesian perception*: Next, we assess the perceptual acuity of the fingertip locating a rod with an active method for robot perception. Active Bayesian perception accumulates location belief up to a decision threshold $P(x_t | z_{1:t}) \geq \theta_{\text{dec}}$, as in passive perception; however, in addition, a control policy attempts to relocate the sensor between taps according to these location beliefs. Here we use a ‘fixation point’ policy, in which a best estimate of current location is used to calculate a relative move to a fixed location on the object (example trajectories

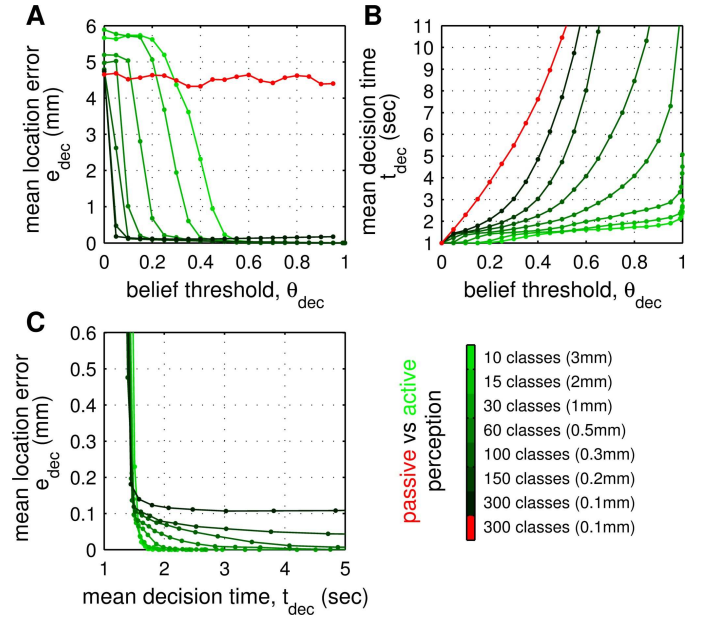


Fig. 11. Location-averaged performance for active and passive perception with the fingertip. (A) Mean errors \bar{e}_{dec} and (B) decision times \bar{t}_{dec} plotted against belief threshold (10000 trials per threshold). Passive perception is shown in red and active perception in green, shaded by location class number N_{loc} . (C) Mean location error plotted against decision time (with threshold an implicit parameter). Active performs better than passive perception, and both improve with increasing belief threshold and decreasing class number.

in Fig. 7B). We take this fixation point in the center of the fingertip’s location range ($x_{\text{fix}} = 15$ mm), where the passive perception had good acuity. The range of decision thresholds $\theta_{\text{dec}} = 0-0.999$ remains unchanged from the previous section, to permit comparison of the active and passive approaches.

Active perceptual decisions of object location are again started from random locations, so we measure performance by the mean perceptual error \bar{e}_{dec} over all initial contact locations (Fig. 11; green plots). The best accuracies were for the higher belief thresholds (Fig. 11A) corresponding to decision times greater than two taps (Fig. 11C). Even for two taps, the active perception reaches a mean error $\bar{e}_{\text{dec}} \lesssim 0.12$ mm, an order of magnitude better than passive perception (~ 4.5 mm) and the (4 mm) spacing between taxels (Table II).

Perceptual performance also depends on the number of location classes, considered over $N_{\text{loc}} = 10-300$ with location class resolution $30/N_{\text{loc}}$ mm. Thus, both the mean location error \bar{e}_{dec} and decision time \bar{t}_{dec} depend on the class number and decision threshold, with their variation with threshold more rapid for larger class numbers N_{loc} (Figs 11A,B). This variability partially cancels in the speed-accuracy curves of mean location error against mean decision time (Fig. 11C) until the error falls to an asymptote. The best location error then depends on class number, with mean errors increasing from $\bar{e}_{\text{dec}} = 0.00$ mm (10 classes) to 0.12 mm (300 classes), while class resolution decreases from 3 mm to 0.1 mm (Table II). Thus, location acuity and class resolution become similar for 300 classes, giving a best perceptual acuity of 0.12 mm.

Considering the taxel spacing is 4 mm for the fingertip, active perception gave a localization hyperacuity with greater than thirty-fold improvement over sensor resolution.

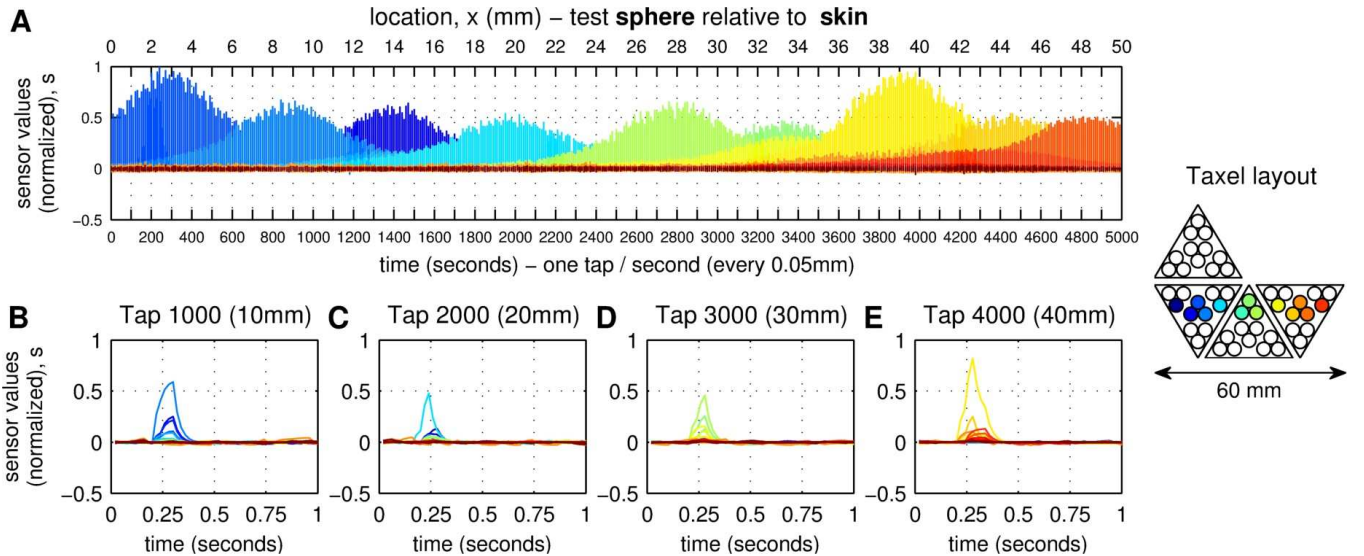


Fig. 12. Tactile data collected as some tactile skin taps against a test sphere (dia. 8 mm) at constant rate of 1 tap/second, with 0.01 mm displacement after every tap to span a 50 mm range with 5000 taps. (B-E) Individual tap data taken from panel (A). Taxels are colored according to their layout on the skin.

B. Tactile skin

1) *Inspection of raw data:* Data for the tactile skin (Fig. 12) were collected while the sensor tapped vertically onto and off the test object (spherical ball, 8 mm diameter). Each tap was then followed by a move over the sphere to sample across a 50 mm location range. At the beginning of the data collection only the taxels on the center-left of the skin are in contact, then the middle taxels and finally the taxels at the center-right. Each taxel has a broad, Gaussian-shaped receptive field about 16 mm across with centers spaced every 4 mm (Fig. 12A). Individual taps typically took ~ 0.1 sec to reach peak amplitude, followed by rapid decay to baseline (Figs 12B-E). Notable differences between the skin and fingertip data are the larger number of taxels now traversed and their broader receptive fields.

The pattern of taxel pressures and their response amplitudes depend on the location of skin relative to the test sphere (similarly to the fingertip and rod), permitting classification of where the sphere is located relative to the skin.

2) *Passive Bayesian perception:* The perceptual acuity of the skin for locating the sphere is assessed first with the same passive Bayesian method for robot perception that was applied to the fingertip and rod. Results are again generated with a Monte Carlo procedure (Sec. III-C), such that each contact tap *passively* remains at its initial location class.

Passive perceptual decisions of object location are evaluated for decision thresholds θ_{dec} from 0-0.999, over $N_{loc} = 50$ location classes spanning the 50 mm range across the skin (Fig. 13). Perception is generally of sub-taxel accuracy across

this range, with mean location errors $e_{dec} \lesssim 1$ mm (Fig. 13A), other than a few regions where the location error increases (e.g. the extremities, as with the fingertip). The decision errors are highly variable, with some locations giving near perfect accuracy $e_{dec} \sim 0$ mm and others poor accuracy $e_{dec} \sim 1$ mm, as also for the mean decision times (Fig. 10B). We attribute this variability to the choice of test object: the spherical stimulus usually has a strong contact on just one taxel, unlike the rod that has strong contacts over multiple taxels. Hence, less information is available for localization with the sphere, apart from at ‘sweet spots’ where it happens to hit multiple taxels; for example, the region 35-38 mm activates several taxels (Fig. 12) with small errors and decision times (Fig. 13).

A typical localization accuracy for passive perception with the skin and sphere is a mean \bar{e}_{dec} over all possible sensing locations (Fig. 14A, red plot). This mean location error $\bar{e}_{dec} \sim 0.4$ mm is consistent with the 0-1 mm location error variability described above. In comparison with the rod and fingertip (Sec. IV-A2), the location acuity is finer because the poor acuity at the extremities is limited to a smaller proportion of the overall range. That being said, we still expect that the perceptual performance can be improved by utilizing regions of relatively good acuity within the location range.

3) *Active Bayesian perception:* The acuity of the tactile skin locating a sphere is now assessed with the same active method for robot perception that was applied to the fingertip and rod. Again we use a ‘fixation point’ policy, in which a best estimate of current location is used to calculate a relative move

number of classes, N_{loc}	25	50	100	200	250	500
class width, x_{class}	2 mm	1 mm	0.5 mm	0.35 mm	0.2 mm	0.1 mm
mean decision error, \bar{e}_{dec} (passive perception)	0.4 mm					
mean decision error, \bar{e}_{dec} (active perception)	0.01 mm	0.05 mm	0.11 mm	0.20 mm	0.18 mm	0.24 mm
acuity, $\max(x_{class}, \bar{e}_{dec})$ (active perception)	2 mm	1 mm	0.5 mm	0.25 mm	0.20 mm	0.24 mm

TABLE III

ACTIVE PERCEPTUAL ACUITY DEPENDS ON LOCATION CLASS WIDTH. RESULTS ARE FOR MEAN DECISION TIMES OF 4 TAPS.

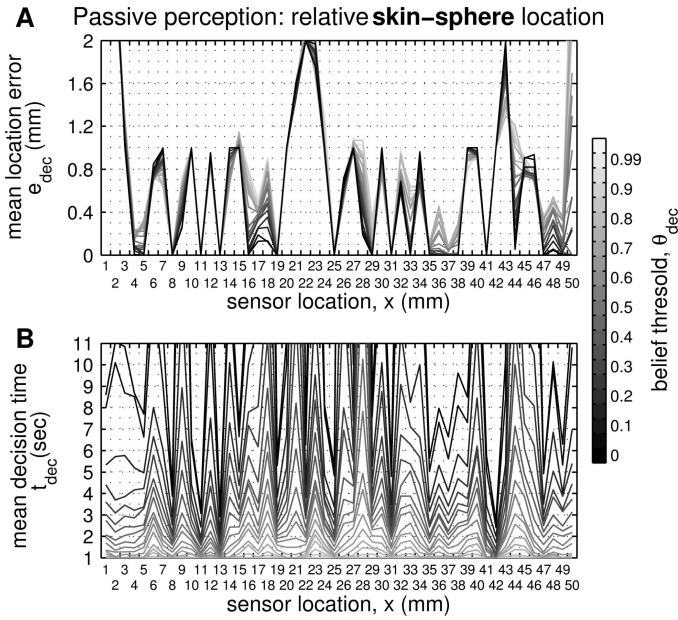


Fig. 13. Acuity of passive Bayesian perception depends on relative skin-sphere location and belief threshold. (A) Mean location error e_{dec} and (B) mean decision time t_{dec} plotted against sensor location, with the gray-scale denoting belief threshold (10000 trials per threshold value, with $N_{\text{loc}} = 50$ location classes). Perceptual performance varies across the location range, with only some regions having consistently good performance (e.g. 35-38 mm).

to a fixed location on the object. We take this fixation point within the ‘sweet spot’ noted above ($x_{\text{fix}} = 37$ mm) where the passive perception had the best acuity. The range of decision thresholds $\theta_{\text{dec}}=0-0.999$ remains unchanged from above, to permit comparison of the active and passive approaches.

As in previous sections, we measure perceptual performance by the mean error \bar{e}_{dec} over all initial contact locations (Fig. 14; green plots). The best accuracies were again for the higher belief thresholds (Fig. 14A) corresponding to decision times greater than 4-5 taps (Fig. 14C). Then active perception reaches an accuracy $\bar{e}_{\text{dec}} \lesssim 0.25$ mm, finer than passive perception (~ 0.4 mm) and the (4 mm) taxel spacing (Table III).

Perceptual performance again depends on the number of location classes, considered over $N_{\text{loc}} = 25-500$ with location class width $50/N_{\text{loc}}$ mm, and the above-mentioned dependence on decision threshold (Figs 14A,B). The best perceptual errors increase with class number from $\bar{e}_{\text{dec}} = 0.00$ mm (25 classes) to 0.25 mm (500 classes), while class resolution improves from 2 mm to 0.1 mm (Table III). Location accuracy and class resolution become similar for 250 classes, giving a best perceptual acuity of 0.20 mm.

Considering the taxel spacing is 4 mm for the skin, active perception gives a localization hyperacuity with twenty-fold improvement in acuity over sensor resolution.

V. DISCUSSION

In this study, we demonstrated hyperacuity with a tactile fingertip and a region of tactile skin: for the fingertip localizing a rod, the best acuity was 0.12 mm, a thirty-fold improvement over the (4 mm) sensor resolution; for the skin localizing a sphere, the best acuity was 0.20 mm, a twenty-fold improvement over sensor resolution. This hyperacuity is comparable

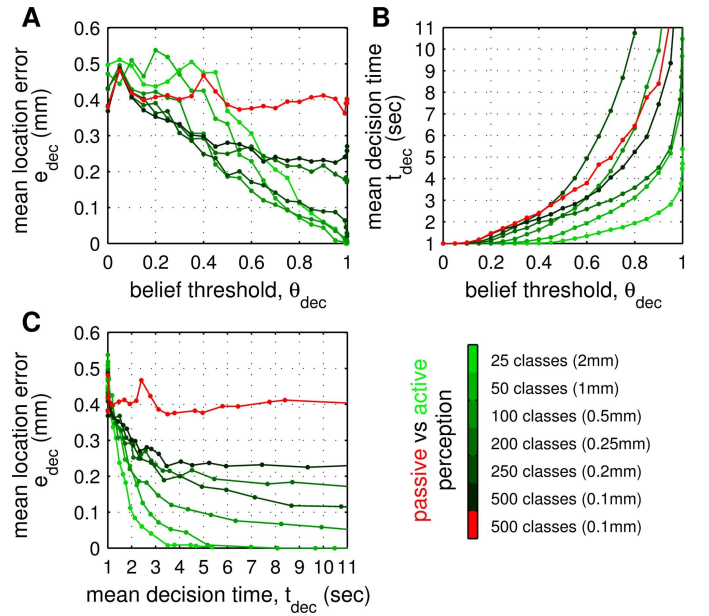


Fig. 14. Location-averaged performance for active and passive perception with the tactile skin. (A) Mean localization errors \bar{e}_{dec} and (B) decision times \bar{t}_{dec} plotted against belief threshold (10000 trials per threshold). Passive perception is shown in red and active perception in green. (C) Mean perceptual error against decision time. Active performs better than passive perception, and both improve with increasing belief threshold and decreasing class number.

with that obtained in human vision and touch, of about 1-2 orders of magnitude better than the sensory receptor spacing. A combination of factors are necessary to attain this degree of hyperacuity, both in the design of the tactile sensors and the methods for robot touch, which we now discuss.

A. Design of the tactile sensor

The construction of the tactile sensor is crucial for attaining hyperacuity. Both the tactile fingertip and skin used here have a taxel-based design with the following key properties (see Figs 9,12): (i) the taxel receptive fields (areas sensitive to contact) are broader than the taxel spacing; (ii) the taxel contact sensitivity peaks in the center of the taxel and decreases gradually away from that peak; (iii) the taxels have good contact pressure resolution, as evident in the smooth change in contact sensitivity across the receptive field. The importance of these properties is that a contact against the tactile sensor will be encoded across multiple taxels, with pressure readings that change smoothly and gradually with small changes in contact location. In consequence, location is represented within the contact data at a finer precision than the taxel spacing, *i.e.* the sensor resolution, which appropriate computational methods can utilize to attain hyperacuity.

We are aware of other tactile sensors with similar response properties, which may also have the potential for localization hyperacuity. For example, the TakkTile is a strip of MEMS barometer chips covered in rubber, having broad overlapping receptive fields with sensitivity to contact location that decreases from a central peak [31, Fig. 8]; another MEMS-based sensor designed for a robotic finger has similar response characteristics [32] and is similarly likely to attain hyperacuity.

A biomimetic fingertip with soft tissue, bone and embedded force sensors also has broad, overlapping receptive fields [33, Fig. 9]. Although we have not seen their response characteristics, we expect various taxel-based tactile sensors should also have appropriate receptive field properties for hyperacuity; for example, the Biotac [34], DLR artificial skin [35] and the capacitive tactile sensors on the Schunk and Barrett hands.

For touch-based applications in future robotics, our expectation is that sensor optimization will be a sophisticated procedure, requiring modeling and empirical studies to customize the design to suit a robot's intended use. Multiple design characteristics can impact on the sensor performance, including taxel density, spatial layout, pressure sensitivity and receptive field size or shape. These properties will depend non-trivially on the morphology of the sensor and its material construction; for example, a stiff coating would distribute force over a large area, giving broad but insensitive receptive fields. We expect sensor optimization will be a complicated procedure (because of the large number of variables), although some recent developments in robot touch could ease this process. In particular, 3D-printed tactile sensors [36], [37] could accelerate the design-testing cycle for sensor customization, while finite element modeling of tactile sensors has the potential to enable a primarily simulation-based design process [38], [39].

B. Computational method for perception

The tactile perception method is also crucial for attaining hyperacuity, because it must interpolate between multiple taxels to localize at a finer acuity than the taxel spacing. We used a statistical method of Bayesian perception that is grounded in optimal decision making and perceptual neuroscience [20]–[22], [28]. Two aspects of Bayesian perception help it attain hyperacuity. First, the method is based on sequential analysis methods for optimal decision making under uncertainty, leading to an optimal tradeoff between the costs of making localization errors and gathering more data [29]. Second, our implementation makes a simplifying assumption of statistical independence between sensor readings to fuse measurements in a simple yet statistically robust manner. Thus, evidence from distinct taxels is fused to estimate contact location over many taxels and evidence from distinct tactile contacts is fused to further improve location acuity.

Algorithmic methods for hyperacuity have been confined mainly to image processing (see background in Sec. II-B), where it is known as *geometrical superresolution* [13], [16]. There are two main applications: deblurring, achieved with signal processing methods such as inverse spatial filtering, and sub-pixel localization, achieved with statistical methods that estimate the centroid of a light distribution. The latter techniques relate more closely to our approach; for example, superresolution fluorescence microscopy combines evidence for the location of fluorescent proteins over many photons (and was the Nature 2008 ‘Method of the Year’ [18]).

Image processing methods are beginning to be adopted in robot touch for sensors with large taxel arrays. Ho *et al* locate the position and orientation of objects using image moments over a 44×44 taxel array [40], and we would expect such

methods to achieve hyperacuity with suitable stimuli; indeed, related methods for tactile servoing with a 16×16 array can reach sub-taxel resolution [41, Fig. 2]. It is important to contrast such image-based tactile sensing methods, which rely on large numbers of activated taxels, with the perception-based methods applied here, which also apply to sensors with few taxels (*e.g.* 12 taxels for the tactile fingertip). The suitability of these methods and their relation to sensor design is an open research topic, but we expect a key consideration will be their integration with active control during perception.

C. Active perception

The final factor necessary for robust tactile hyperacuity is to use active control during perception. Our Bayesian perception method extends naturally to active perception by moving the sensor with a control strategy based on evidence received during the localization decision. Benefits of active Bayesian perception include: (i) an order-of magnitude improvement in acuity over passive methods [8], [25], [27]; (ii) robust perception in unstructured environments [25]; and (iii) relation to a general framework for simultaneous object localization and identification [8]. In consequence, a thirty-fold improvement in perceptual acuity (from 4 mm to 0.12 mm) is obtained using an active control policy that centers the tactile fingertip on the rod, enabling robust hyperacuity.

To the best of our knowledge, the connection between active perception and hyperacuity has not been emphasized in the biology or engineering literatures. The main point is that perceptual acuity depends on how a sensor interacts with an object, which must thus be actively controlled to attain the best acuity. For example, in robot touch, the perceptual acuity is known to vary strongly with contact location [4], [8], [25], and thus passive perception performs badly when that contact location cannot be set *a priori*. This dependence between acuity and control is a general aspect of biological and artificial perception [42], from eye movements that perform visual tasks such as smooth pursuit, to actively controlling our fingers and hands for exploring and recognizing objects [43].

VI. CONCLUSION

In this paper, we proposed that hyperacuity should be a central consideration for the design and application of artificial tactile sensors, just as it a fundamental aspect of biological perception. Tactile hyperacuity depends on three key factors: *sensor design*, to have multiple, overlapping, broad but sensitive receptive fields; *perceptual inference* that interpolates between these overlapping receptors to perceive at sub-taxel acuity; and *active perception*, to ensure robustness of the perception in unstructured environments. We envisage that these principles could become central to the construction and deployment of cheap yet high-acuity tactile sensors, which could be individually customized so that their design optimally matches their intended application in robot touch.

REFERENCES

- [1] G. Westheimer, “Visual acuity and hyperacuity,” *Investigative Ophthalmology*, vol. 14, no. 8, pp. 570–572, 1975.

- [2] J. Loomis, "An investigation of tactile hyperacuity," *Sensory Processes*, vol. 3, pp. 289–302, 1979.
- [3] J. M. Loomis, "On the tangibility of letters and braille," *Perception & Psychophysics*, vol. 29, no. 1, pp. 37–46, 1981.
- [4] N. Lepora, U. Martinez-Hernandez, H. Barron-Gonzalez, M. Evans, G. Metta, and T. Prescott, "Embodied hyperacuity from bayesian perception: Shape and position discrimination with an icub fingertip sensor," in *Intelligent Robots and Systems (IROS), 2012 IEEE/RSJ International Conference on*, 2012, pp. 4638–4643.
- [5] A. Schmitz, P. Maiolino, M. Maggiali, L. Natale, G. Cannata, and G. Metta, "Methods and technologies for the implementation of large-scale robot tactile sensors," *IEEE Trans Robotics*, vol. 27, no. 3, pp. 389–400, 2011.
- [6] G. Metta, G. Sandini, D. Vernon, L. Natale, and F. Nori, "The icub humanoid robot: an open platform for research in embodied cognition," in *Proc. 8th Workshop on Intelligent Systems*, 2008, pp. 50–56.
- [7] G. Cannata, M. Maggiali, G. Metta, and G. Sandini, "An embedded artificial skin for humanoid robots," in *Multisensor Fusion and Integration for Intelligent Systems, 2008. MFI 2008. IEEE International Conference on*. IEEE, 2008, pp. 434–438.
- [8] N. Lepora, U. Martinez-Hernandez, and T. Prescott, "Active bayesian perception for simultaneous object localization and identification," in *Robotics: Science and Systems*, 2013.
- [9] R. Dahiya, G. Metta, M. Valle, and G. Sandini, "Tactile sensing - from humans to humanoids," *Robotics, IEEE Transactions on*, vol. 26, no. 1, pp. 1–20, 2010.
- [10] G. Westheimer, "Visual acuity and hyperacuity," *Handbook of Optics, Vol. III: Vision and Vision Optics*, pp. 4–1, 2009.
- [11] Wikipedia, "Hyperacuity (scientific term) — Wikipedia, the free encyclopedia," 2013.
- [12] N. McWhirter, *The Guinness Book of World Records 1985*. Sterling Publishing Company, 1985, entry for "highest hyperacuity" (Dr D. Levi).
- [13] G. Westheimer, "Optical superresolution and visual hyperacuity," *Progress in Retinal and Eye Research*, vol. 31, no. 5, pp. 467–480, 2012.
- [14] Q. Tian and M. N. Huhns, "Algorithms for subpixel registration," *Computer Vision, Graphics, and Image Processing*, vol. 35, no. 2, pp. 220–233, 1986.
- [15] P. Debevec and J. Malik, "Recovering high dynamic range radiance maps from photographs," in *SIGGRAPH 97, Conference Proceedings*, 1997, pp. 369–378.
- [16] Z. Zalevsky and D. Mendlovic, *Optical superresolution*. Springer, 2004, vol. 91.
- [17] V. Marx, "Is super-resolution microscopy right for you?" *Nature Methods*, vol. 10, no. 12, pp. 1157–1163, 2013.
- [18] Editorial, "Method of the year 2008," *Nature Methods*, vol. 6, p. 1, 2009.
- [19] N. Lepora, J. Sullivan, B. Mitchinson, M. Pearson, K. Gurney, and T. Prescott, "Brain-inspired bayesian perception for biomimetic robot touch," in *Robotics and Automation (ICRA), 2012 IEEE International Conference on*, 2012, pp. 5111–5116.
- [20] N. Lepora, C. Fox, M. Evans, M. Diamond, K. Gurney, and T. Prescott, "Optimal decision-making in mammals: insights from a robot study of rodent texture discrimination," *Journal of The Royal Society Interface*, vol. 9, no. 72, pp. 1517–1528, 2012.
- [21] R. Bogacz and K. Gurney, "The basal ganglia and cortex implement optimal decision making between alternative actions," *Neural computation*, vol. 19, no. 2, pp. 442–477, 2007.
- [22] N. Lepora and K. Gurney, "The basal ganglia optimize decision making over general perceptual hypotheses," *Neural Computation*, no. 24, pp. 2924–2945, 2012.
- [23] M. Evans, C. Fox, M. Pearson, N. Lepora, and T. Prescott, "Whisker-object contact speed affects radial distance estimation," in *Robotics and Biomimetics (ROBIO)*, 2010, pp. 720–725.
- [24] M. H. Evans, C. W. Fox, N. F. Lepora, M. J. Pearson, J. C. Sullivan, and T. J. Prescott, "The effect of whisker movement on radial distance estimation: a case study in comparative robotics," *Frontiers in Neuro-robotics*, vol. 6, 2012.
- [25] N. Lepora, U. Martinez-Hernandez, and T. Prescott, "Active touch for robust perception under position uncertainty," in *Robotics and Automation (ICRA), 2013 IEEE International Conference on*, 2013.
- [26] N. Lepora, U. Martinez-Hernandez, G. Pezzulo, and T. Prescott, "Active bayesian perception and reinforcement learning," in *Intelligent Robots and Systems (IROS), 2013 IEEE/RSJ International Conference on*, 2013, pp. 4735–4740.
- [27] N. Lepora, U. Martinez-Hernandez, and T. Prescott, "A SOLID case for active bayesian perception in robot touch," in *Biomimetic and Biohybrid Systems*. Springer Berlin Heidelberg, 2013, pp. 154–166.
- [28] J. Gold and M. Shadlen, "The neural basis of decision making," *Annu. Rev. Neurosci.*, vol. 30, pp. 535–574, 2007.
- [29] A. Wald and J. Wolfowitz, "Optimum character of the sequential probability ratio test," *The Annals of Mathematical Statistics*, vol. 19, no. 3, pp. 326–339, 1948.
- [30] N. Lepora, M. Evans, C. Fox, M. Diamond, K. Gurney, and T. Prescott, "Naive bayes texture classification applied to whisker data from a moving robot," *Neural Networks (IJCNN), The 2010 International Joint Conference on*, pp. 1–8, 2010.
- [31] Y. Tenzer, L. Jentoft, and R. Howe, *Inexpensive and Easily Customized Tactile Array Sensors using MEMS Barometers Chips*, 2012.
- [32] H. Muhammad, C. Oddo, L. Beccai, C. Recchiuto, C. Anthony, M. Adams, M. Carrozza, D. Hukins, and M. Ward, "Development of a bioinspired MEMS based capacitive tactile sensor for a robotic finger," *Sensors and Actuators A: Physical*, vol. 165, no. 2, pp. 221–229, 2011.
- [33] K. Chathuranga, V. Ho, and S. Hirai, "A biomimetic fingertip that detects force and vibration modalities and its application to surface identification," in *Robotics and Biomimetics (ROBIO), 2012 IEEE International Conference on*. IEEE, 2012, pp. 575–581.
- [34] J. Fishel and G. Loeb, "Sensing tactile microvibrations with the bio-tacomparison with human sensitivity," in *Biomedical Robotics and Biomechatronics (BioRob), 2012 4th IEEE RAS & EMBS International Conference on*. IEEE, 2012, pp. 1122–1127.
- [35] M. Strohmayer and D. Schneider, "The DLR artificial skin step II: Scalability as a prerequisite for whole-body covers," in *Intelligent Robots and Systems (IROS), 2013 IEEE/RSJ International Conference on*. IEEE, 2013, pp. 4721–4728.
- [36] C. Chorley, C. Melhuish, T. Pipe, and J. Rossiter, "Development of a tactile sensor based on biologically inspired edge encoding," in *Advanced Robotics, 2009. ICAR 2009. International Conference on*. IEEE, 2009, pp. 1–6.
- [37] B. Winstone, G. Griffiths, C. Melhuish, T. Pipe, and J. Rossiter, "TACTIP - tactile fingertip device, challenges in reduction of size to ready for robot hand integration," in *Robotics and Biomimetics (ROBIO), 2012 IEEE International Conference on*. IEEE, 2012, pp. 160–166.
- [38] T. Le, P. Maiolino, F. Mastrogianni, A. Schmitz, and G. Cannata, "A toolbox for supporting the design of large-scale capacitive tactile systems," in *Humanoid Robots (Humanoids), 2011 11th IEEE-RAS International Conference on*. IEEE, 2011, pp. 153–158.
- [39] V. Ho and S. Hirai, "Modeling and analysis of a frictional sliding soft fingertip, and experimental validations," *Advanced Robotics*, vol. 25, no. 3–4, pp. 291–311, 2011.
- [40] V. Ho, T. Nagatani, A. Noda, and S. Hirai, "What can be inferred from a tactile arrayed sensor in autonomous in-hand manipulation?" in *Automation Science and Engineering (CASE), 2012 IEEE International Conference on*. IEEE, 2012, pp. 461–468.
- [41] Q. Li, C. Schürmann, R. Haschke, and H. Ritter, "A control framework for tactile servoing," in *Robotics: Science and Systems*, 2013.
- [42] R. Bajcsy, "Active perception," *Proceedings of the IEEE*, vol. 76, no. 8, pp. 966–1005, 1988.
- [43] S. J. Lederman and R. L. Klatzky, "Hand movements: A window into haptic object recognition," *Cognitive psychology*, vol. 19, no. 3, pp. 342–368, 1987.



Nathan F. Lepora received the B.A. degree in Mathematics and the Ph.D. degree in Theoretical Physics from the University of Cambridge, U.K.

He is currently a Lecturer with the Department of Engineering Mathematics, University of Bristol, U.K., and is affiliated with the Bristol Robotics Laboratory, University of Bristol and the University of the West of England, U.K. He is also a honorary research fellow at the Sheffield Center for Robotics and the Department of Psychology, University of Sheffield, U.K., where he was a Research Associate

then Research Fellow from 2005–2013. He has been program chair for the International Conference 'Living Machines' in 2012 and 2013. His research interests span robotics and computational neuroscience, focussing on robot and animal perception, artificial and natural decision making, and biomimetics.



Uriel Martínez-Hernández received the B.Sc. degree in Communications and Electronics from the Instituto Politecnico Nacional, Mexico City, Mexico in 2005 and the M.Sc. degree in Computer Sciences from the Centro de Investigación y de Estudios Avanzados del Instituto Politecnico Nacional, Mexico City, Mexico in 2008.

He is working towards a Ph.D. degree in Automatic Control and Systems Engineering from the University of Sheffield, Sheffield, U.K. His research interests include robot perception and control.



Mat Evans received the B.Sc. degree in Psychology, M.Sc in Computational and Systems Neuroscience, and the Ph.D. degree in Robotics from the University of Sheffield, U.K.

He is currently a Research Associate and member of the Active Touch Laboratory at the University of Sheffield, interested in the processing that underlies active sensing.



Lorenzo Natale received the Electronic Engineering degree (with honors) and the Ph.D. degree in robotics from the University of Genoa, Italy, in 2000 and 2004.

He was with the Laboratory for Integrated Advanced Robotics, University of Genoa. Between 2005 and 2006, he was a Postdoctoral Researcher with the Humanoid Robotics Group, Computer Science and Artificial Intelligence Laboratory, Massachusetts Institute of Technology, Cambridge. He is currently a Team Leader with the Italian Institute

of Technology, Genoa. His current research interests include developmental robotics, sensorimotor learning, and perception in artificial and biological systems, as well as software development and integration in robotics.



Giorgio Metta received the M.S. degree (Hons.) in 1994 and the Ph.D. degree in 2000, both in electronic engineering, from the University of Genoa, Italy.

From 2001 to 2002, he was a Postdoctoral Associate with the Artificial Intelligence Laboratory, Massachusetts Institute of Technology, Cambridge. He has been an Assistant Professor with the Dipartimento di Informatica Sistemistica e Telematica, University of Genoa, since 2005. Since 2006, he has also been a Senior Scientist with the Robotics, Brain, and Cognitive Sciences Department, Italian Institute

of Technology, Genoa. His current research interests include biologically motivated humanoid robotics and, in particular, the development of artificial systems that show some of the abilities of natural systems. He is the author of more than 100 publications, and also engaged as a Principal Investigator and Research Scientist in several international and national funded projects.



Tony J. Prescott received the M.A. degree in psychology from University of Edinburgh, Edinburgh, U.K., the M.Sc. degree in Artificial Intelligence from the University of Aberdeen, Aberdeen, U.K., and the Ph.D. degree from the Department of Psychology, University of Sheffield, Sheffield, U.K., in 1994.

He is currently a Professor of cognitive neuroscience with the Department of Psychology, University of Sheffield. He is also a Permanent Research Fellow with the Bristol Robotics Laboratory, Bristol, U.K. He has authored more than 60 publications in

psychology, neuroscience, computational modeling and robotics. His research interests include the biological and brain sciences, particularly concerned with understanding the evolution, development, and function of natural intelligence and the investigation of computational neuroscience models of animal and human intelligence and in testing these models in biomimetic robots.